AD-A047 627 ILLINOIS UNIV AT URBANA-CHAMPAIGN COORDINATED SCIENCE LAB F/G 20/3
A NEW LOOK AT THE SCATTERING OF A PLANE WAVE BY RECTANGULAR CYL--ETC(U).
JUL 77 W L KO, R MITTRA DAAB07-72-C-0259
UNCLASSIFIED R-776 NL

1 OF 1
AD
A047627

END
DATE
FILMED
1-78
DDC

AD A047627

REPORT R-776 JULY, 1977 UILU-ENG 77-2223

CSL COORDINATED SCIENCE LABORATORY

A NEW LOOK AT THE SCATTERING OF A PLANE WAVE BY A RECTANGULAR CYLINDER

W. L. KO
R. MITTRA

AD No.
DDC FILE COPY

DISTRIBUTION STATEMENT A
Approved for public release;
Distribution Unlimited

DDC
RECEIVED
DEC 14 1977
B

UNIVERSITY OF ILLINOIS - URBANA, ILLINOIS

UNCLASSIFIED

SECURITY CLASSIFICATION OF THIS PAGE (When Data Entered)

REPORT DOCUMENTATION PAGE		READ INSTRUCTIONS BEFORE COMPLETING FORM
1. REPORT NUMBER	2. GOVT ACCESSION NO.	3. RECIPIENT'S CATALOG NUMBER
4. TITLE (and Subtitle) (6) A NEW LOOK AT THE SCATTERING OF A PLANE WAVE BY A RECTANGULAR CYLINDER,		5. TYPE OF REPORT & PERIOD COVERED (9) Technical Report,
		6. PERFORMING ORG. REPORT NUMBER (14) R-776, UILU-ENG-77-2223
7. AUTHOR(s) (10) W. L. Ko and R. Mittra		8. CONTRACT OR GRANT NUMBER(s) (15) DAAB-07-72-C-0259, ARO DAAG29-77-G-0111
9. PERFORMING ORGANIZATION NAME AND ADDRESS Coordinated Science Laboratory University of Illinois at Urbana-Champaign Urbana, Illinois 61801		10. PROGRAM ELEMENT, PROJECT, TASK AREA & WORK UNIT NUMBERS
11. CONTROLLING OFFICE NAME AND ADDRESS Joint Services Electronics Program (11)		12. REPORT DATE July, 1977
		13. NUMBER OF PAGES 34
14. MONITORING AGENCY NAME & ADDRESS(if different from Controlling Office) (12) 38p.		15. SECURITY CLASS. (of this report) UNCLASSIFIED
		15a. DECLASSIFICATION/DOWNGRADING SCHEDULE

16. DISTRIBUTION STATEMENT (of this Report)

Approved for public release; distribution unlimited

17. DISTRIBUTION STATEMENT (of the abstract entered in Block 20, if different from Report)

18. SUPPLEMENTARY NOTES

19. KEY WORDS (Continue on reverse side if necessary and identify by block number)

High Frequency Scattering
Rectangular Cylinder
Spectral Domain Approach
Asymptotic Methods

20. ABSTRACT (Continue on reverse side if necessary and identify by block number)

In this paper, the scattered far-field pattern of a perfectly conducting rectangular cylinder illuminated by a plane H-wave is obtained by a modified form of GTD approximation and the result is subsequently improved in a straightforward manner by eliminating the discontinuities in the GTD far-field pattern. The improved scattered far-field pattern is compared with results obtained by other different approaches, and the similarities and differences between these results are discussed. Generally speaking, the improved →

DD FORM 1 JAN 73 1473 EDITION OF 1 NOV 65 IS OBSOLETE

UNCLASSIFIED

SECURITY CLASSIFICATION OF THIS PAGE (When Data Entered)

097 700

20. ABSTRACT (continued)

pattern obtained by the present approach is in good agreement with the conventional moment-method solution. A method for checking the accuracy is also presented so that an independent check on the satisfaction of the boundary condition on the surface of the rectangular cylinder can be performed. The results of such an accuracy check are quite favorable, which demonstrates that the improved far-field pattern obtained by the present approach is indeed a close approximation to the true solution. The merit of such an independent accuracy checking scheme is that the approximate solution obtained can be validated without making comparison with other methods.

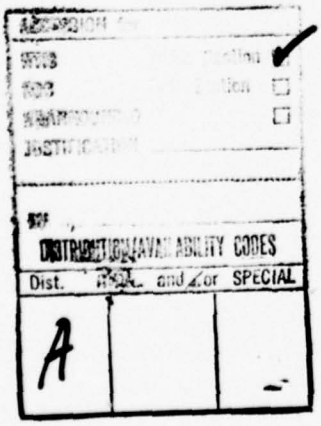

UILU-ENG 77-2223

A NEW LOOK AT THE SCATTERING OF A PLANE WAVE BY A RECTANGULAR CYLINDER

by

W. L. Ko and R. Mittra

This work was supported in part by the Joint Services Electronics Program (U.S. Army, U.S. Navy and U.S. Air Force) under Contract DAAB-07-72-C-0259 and in part by the Army Research Office under Grant ARO-DAAG-29-77-G-0111.

Reproduction in whole or in part is permitted for any purpose of the United States Government.

Approved for public release. Distribution unlimited.

A NEW LOOK AT THE SCATTERING OF A PLANE WAVE BY A RECTANGULAR CYLINDER

by

W. L. Ko and R. Mittra
Electromagnetics Laboratory
Department of Electrical Engineering
University of Illinois at Urbana-Champaign
Urbana, Illinois 61801

ABSTRACT

In this paper, the scattered far-field pattern of a perfectly conducting rectangular cylinder illuminated by a plane H-wave is obtained by a modified form of GTD approximation and the result is subsequently improved in a straightforward manner by eliminating the discontinuities in the GTD far-field pattern. The improved scattered far-field pattern is compared with results obtained by other different approaches, and the similarities and differences between these results are discussed. Generally speaking, the improved pattern obtained by the present approach is in good agreement with the conventional moment-method solution. A method for checking the accuracy is also presented so that an independent check on the satisfaction of the boundary condition on the surface of the rectangular cylinder can be performed. The results of such an accuracy check are quite favorable, which demonstrates that the improved far-field pattern obtained by the present approach is indeed a close approximation to the true solution. The merit of such an independent accuracy checking scheme is that the approximate solution obtained can be validated without making comparison with other methods.

1. INTRODUCTION

The problem of scattering of electromagnetic waves by a rectangular cylinder has been investigated by numerous scientific researchers in the past; yet the interest in this problem is still strong, as evidenced by a rather large number of papers that have recently appeared in the literature [1], [2], [3], [4], [5], [6] on this subject.

Due to its two-dimensional nature, the conventional moment method [2] can be applied to this problem even when the cylinder is electrically large, particularly when its symmetric properties are fully exploited. Therefore, it provides a convenient validity check for other methods. Indeed, Burnside et al. [1] and Mautz et al. [3] have claimed the validity of their solutions only by a comparison of their results with the conventional moment method.

Both of the aforementioned papers employ the so-called uniform geometrical theory of diffraction developed by Kouyoumjian et al. [7] in which the classical wedge diffraction coefficient put forth by Keller is modified using multiplicative factors in such a manner that one of these factors goes to zero as the Keller's diffraction coefficient goes to infinity at one of the shadow or reflection boundaries so that the product remains finite. The resulting diffraction coefficient is indeed applicable at all aspect angles. It is conceivable that an additive term which goes to infinity as the Keller's diffraction coefficient goes to infinity, but with opposite sign, will work equally well as does the multiplicative-factor type of remedy. Indeed, this additive-term type of remedy has been followed by Lewis et al. [8] and has been investigated by a number of other workers [8].

In this paper, we tackle the scattering problem using a completely different technique which is based on a representation of the scattered

fields in terms of the spectrum of the induced surface current on the scatterer rather than the rays emanating from it. This spectral domain interpretation of high-frequency diffraction phenomena has been documented in detail in a recent paper by Mittra, Rahmat-Samii and Ko [9]. Ko and Mittra [10] also developed a method based on the spectral domain concept for combining the asymptotic high-frequency technique and the integral equation formulation. The method has been applied successfully to infinitesimally thin scattering objects, e.g., an infinite perfectly conducting strip and a finite perfectly conducting square plate [10]. In this paper we illustrate the application of this method to the problem of a perfectly conducting rectangular cylinder. We show that, starting out with Keller's wedge diffraction coefficient, only one iteration gives a far-field pattern that compares extremely well with that obtained from the moment-method solution.

Before closing this section, it is worth mentioning that the GTD result deviates significantly in those directions which coincide with the orientations of the surfaces of the rectangular cylinder even when multiple-edge interactions are included in a self-consistent manner by introducing eight unknown diffraction coefficients. Only when one further modifies the GTD method with the uniform diffraction coefficient and combines it with the moment method using a total of twenty-four unknowns will the result compare well with the moment-method solution for thirty-two unknowns.

2. FORMULATION

The geometry of the electromagnetic scattering problem involving a perfectly conducting infinite rectangular cylinder of cross section $2a \times 2b$ illuminated by a uniform plane wave, whose magnetic intensity vector is oriented parallel to the edges of the cylinder, is depicted in Fig. 1. For convenience of analysis, an arbitrary incident wave can always be decomposed

into two components with respect to the z-axis, namely, TM_z (E-wave) and TE_z (H-wave). In the following discussion we consider the H-wave case only; the E-wave case can be solved in a similar manner by considering $\bar{E}^i = \hat{z}E_0^i$.

In the H-wave case, the incident H-field is given by

$$H_z^i(\rho,\phi) = e^{-ik(x\cos\phi_0+y\sin\phi_0)} \tag{1}$$

where the $e^{-i\omega t}$ time dependence is understood. The geometrical optics reflected field can be derived easily from (1) once the geometrical configuration is known. Hence, the geometrical optics part of the total field will not be discussed further.

We now turn to the diffracted field which results from the sharp edges on the scattering cylinder. As alluded to in Section 1, we make use of the Keller wedge diffraction coefficient to find the diffracted fields. To make this discussion as self-contained as possible and to introduce the notations that we have adopted in this paper, a brief review of the wedge diffraction coefficient is in order.

The geometry of a perfectly conducting wedge immersed in a uniform H-wave in the canonical wedge diffraction problem is shown in Fig. 2. According to Keller's geometrical theory of diffraction, the diffracted field by the edge of the wedge can be constructed by the following formula:

$$H_z^d \sim H_z^i(\text{at the edge of the wedge})\, D_h \frac{e^{ik\rho}}{\sqrt{\rho}}\, (e^{-i\omega t}) \tag{2}$$

where

$$D_h = \frac{e^{i\pi/4}}{\sqrt{2\pi k}} \left[\frac{\frac{1}{n}\sin\frac{\pi}{n}}{\cos\frac{\pi}{n} - \cos\left(\frac{\phi_w - \phi_{0w}}{n}\right)} + \frac{\frac{1}{n}\sin\frac{\pi}{n}}{\cos\frac{\pi}{n} - \cos\left(\frac{\phi_w - \phi_{0w}}{n}\right)} \right] \tag{3}$$

and ~ means "asymptotically equal to." In the above formula, $n\pi$ denotes the exterior region while $(2 - n)\pi$ denotes the wedge angle. Note that n is not necessarily an integer; in the rectangular cylinder case, it will take on the value 3/2. The subscript w attached to the angle of incidence ϕ_0 and the angle of diffraction ϕ serves as a reminder that these angles are used in the canonical problem and their senses are defined as shown in Fig. 2. This fact is worth emphasizing since it is crucial in constructing the diffracted field when several wedges are involved in a scattering problem.

As shown in Fig. 3, the major contributions to the diffracted field are from wedges 1, 2, and 3 since the three edges of these wedges are being illuminated by the incident field whereas wedge 4 is in the dark and, hence, can be ignored in the zeroth-order approximation to the diffracted field. With this in mind, the diffracted far field can be written in a concise fashion as follows:

$$H_z^d(\rho,\phi) \sim \begin{cases} H_{z1}^d\left(\begin{matrix}\phi_w = \phi \\ \phi_{0w} = \phi_0\end{matrix}\right) + H_{z2}^d\left(\begin{matrix}\phi_w = \pi - \phi \\ \phi_{0w} = \pi - \phi_0\end{matrix}\right) + H_{z3}^d\left(\begin{matrix}\phi_w = \pi/2 - \phi \\ \phi_{0w} = \pi/2 - \phi_0\end{matrix}\right) & , 0<\phi<\frac{\pi}{2} \\ H_{z1}^d\left(\begin{matrix}\phi_w = \phi \\ \phi_{0w} = \phi_0\end{matrix}\right) + H_{z2}^d\left(\begin{matrix}\phi_w = \pi - \phi \\ \phi_{0w} = \pi - \phi_0\end{matrix}\right) & , \frac{\pi}{2}<\phi<\pi \\ H_{z1}^d\left(\begin{matrix}\phi_w = \phi \\ \phi_{0w} = \phi_0\end{matrix}\right) + H_{z3}^d\left(\begin{matrix}\phi_w = \pi/2 + (2\pi-\phi) \\ \phi_{0w} = \pi/2 - \phi_0\end{matrix}\right) & , \pi<\phi<\frac{3\pi}{2} \\ H_{z2}^d\left(\begin{matrix}\phi_w = 3\pi - \phi \\ \phi_{0w} = \pi - \phi_0\end{matrix}\right) + H_{z3}^d\left(\begin{matrix}\phi_w = \pi/2 + (2\pi-\phi) \\ \phi_{0w} = \pi/2 - \phi_0\end{matrix}\right) & , \frac{3\pi}{2}<\phi<2\pi \end{cases} \tag{4}$$

where $\phi_0 = \pi/4$. In the above equation, subscripts 1, 2, and 3 on H_z^d designate wedges 1, 2, and 3, respectively. Each of the H_z^d's from the individual wedges is of the form given by (2) and (3) with proper values for ϕ_w and ϕ_{0w} substituted and proper phase shifts taken care of due to the transfer of the phase center, located at the edge of the wedge in each of the individual canonical problems, to the common phase center, located at the origin of the rectangular coordinate system shown in Fig. 3.

2.1 Pole singularities in the diffraction coefficients

It is well-known that the Keller's diffraction coefficient (3) as introduced in the last section will not give the correct value for the diffracted field at certain directions, namely, at the shadow and the reflection boundaries predicted by geometrical optics. One can easily see from (3) that the denominator of either one of the two terms in the square brackets vanishes at one of these shadow and reflection boundaries and gives fictitious, infinite field values at those directions.

Although a number of uniform theories [7], [8] are available for circumventing these difficulties, we suggest a straightforward procedure for accomplishing the same. We note, first of all, that the infinities may be physically interpreted as those associated with physical optics currents with semi-infinite supports [see Reference 11]. Thus we simply subtract the non-physical pole singularities and define a modified diffraction coefficient $\tilde{D}_h$ which is the Keller coefficient minus the pole singularity. With this modification the expression for the diffracted field from wedge 1 (see Fig. 3) becomes

$$H_{z1}^{d} - H_{z}^{i} \text{ (at edge of wedge 1) } \tilde{D}_{h1} \frac{e^{ik\rho}}{\sqrt{\rho}} e^{ika\cos\phi}\, e^{-ikb\sin\phi}$$

$$= e^{-ik(-a\cos\phi_0 + b\sin\phi_0)} \frac{e^{ik\rho}}{\sqrt{\rho}}$$

$$\cdot \frac{e^{i\frac{\pi}{4}}}{\sqrt{2\pi k}} \left[\frac{\frac{2}{3}\sin\frac{2\pi}{3}\, e^{ika\cos\phi}\, e^{-ikb\sin\phi}}{\cos\frac{2\pi}{3} - \cos\frac{2}{3}(\phi - \phi_0)} \right.$$

$$- \frac{e^{ik(a\cos(\pi+\phi_0) - b\sin(\pi+\phi_0))}}{\phi - (\pi + \phi_0)}$$

$$+ \frac{\frac{2}{3}\sin\frac{2\pi}{3}\, e^{ika\cos\phi}\, e^{-ikb\sin\phi}}{\cos\frac{2\pi}{3} - \cos\frac{2}{3}(\phi + \phi_0)}$$

$$\left. - \frac{e^{ik(a\cos(\pi-\phi_0) - b\sin(\pi-\phi_0))}}{\phi - (\pi - \phi_0)} \right] \quad . \tag{5}$$

where

$$0 \le \phi_0 \le \frac{\pi}{2} \text{ and } 0 \le \phi \le \frac{3\pi}{2} \quad .$$

Note that the second term in the square brackets is the pole singularity of the first term at the shadow boundary, and the fourth term is the pole singularity of the third term at the reflection boundary.

Similar expressions for the diffracted fields H_{z2}^{d} and H_{z3}^{d} may be constructed for wedge 2 and wedge 3, respectively, in the appropriate angular regions ($0 \le \phi \le \pi$ and $\frac{3\pi}{2} \le \phi \le 2\pi$ for wedge 2; $0 \le \phi \le \pi/2$ and $\pi \le \phi \le 2\pi$ for wedge 3).

The total diffracted field may now be found by superposing H_{z1}^{d}, H_{z2}^{d} and H_{z3}^{d} as indicated in (4). The far-field pattern computed by using

$\phi_0 = \frac{\pi}{4}$, $a = b = 1\lambda$, in (4) is depicted in Fig. 4. This plot shows that there are no sporadic variations near the shadow and reflection boundaries at 225°, 135°, and 315°. This pattern is already in very good agreement with that obtained by using the moment method, which is shown in Fig. 7. By good agreement, we mean that all the locations of the peaks and nulls are close to the right positions and the levels are more or less correct. Except for the obvious discontinuities in the pattern at the angles of 0°, 90°, 180°, and 270°, which correspond to the directions in which the four surfaces of the rectangular cylinder are oriented, it is really remarkable how good a far-field pattern can be constructed with only a straightforward modification of the zeroth-order GTD solution. A simple physical interpretation for the existence of these discontinuities can be found and their elimination is discussed in the following sections.

Before closing this section, it is noteworthy that, due to the complete symmetry of the rectangular cylinder, the pole singularities in the wedge diffraction coefficients need not be subtracted out explicitly as done in (5) before we use them to compute the far field. In other words, the wedge diffraction coefficient as given in its original form shown in (3) could have been used directly to compute the far-field pattern. While it is admittedly a happy coincidence that the Keller's diffraction coefficients can be used directly in the rectangular cylinder problem, in more general cases the procedure of subtracting pole singularities explicitly from the diffraction coefficient, as done in (5), should be followed in order to get meaningful results near the shadow and the reflection boundaries.

2.2 Discontinuities in the far-field pattern at $\phi = 0, \frac{\pi}{2}, \pi$, and $\frac{3\pi}{2}$

In the previous sections the problem of diffraction by a rectangular cylinder was solved by using modified Keller's wedge diffraction coefficients.

Although the far-field pattern varies smoothly and remains finite across the shadow and reflection boundaries, there are noticeable discontinuities in the pattern at $\phi = 0, \frac{\pi}{2}, \pi$, and $\frac{3\pi}{2}$. These directions are those in which the surfaces of the rectangular cylinder are oriented. In the next section, a physical interpretation of the existence of these discontinuities is given. Before doing that, these discontinuities are explicitly evaluated in this section.

Let us refer to (4). The discontinuity in the far field at $\phi = 0$ is

$$H_z^d(\phi = 0) - H_z^d(\phi = 2\pi)$$

$$= \frac{e^{i\frac{\pi}{4}}}{\sqrt{2}} \frac{e^{ik\rho}}{\sqrt{\pi k\rho}} \left[e^{-ik(-a\cos\phi_0 + b\sin\phi_0)} \frac{(2)(\frac{2}{3}\sin\frac{2\pi}{3})\, e^{ika}}{\cos\frac{2\pi}{3} - \cos\frac{2}{3}\phi_0} \right] . \qquad (6)$$

Following the same lines, the discontinuities in the far field at $\phi = \frac{\pi}{2}, \pi$, and $\frac{3\pi}{2}$ can also be obtained explicitly [11].

2.3 Physical interpretation of the existence of the discontinuities in the far-field pattern at $\phi = 0, \frac{\pi}{2}, \pi$, and $\frac{3\pi}{2}$

In the last section, the discontinuities in the far field at $\phi = 0, \frac{\pi}{2}, \pi$, and $\frac{3\pi}{2}$ have been studied and documented. The fact that the GTD solution of the far field contains discontinuities is well-known. The cause of the existence of these discontinuities is investigated and a simple physical interpretation is given which, in turn, provides a clue to their elimination.

Note that in (4) the far field H_z^d is constructed by using H_{z1}^d, H_{z2}^d, and H_{z3}^d, each of which has its own angular domain of definition. More explicitly, H_{z1}^d is defined on the angular range $0 \leq \phi \leq \frac{3\pi}{2}$ (see Fig. 5a); outside of this angular range, H_{z2}^d is simply assumed to be zero. Likewise,

H^d_{z2} is defined on $0 \leq \phi \leq \pi$ and $\frac{3\pi}{2} \leq \phi \leq 2\pi$ (see Fig. 5b), and H^d_{z3} is on $0 \leq \phi \leq \frac{\pi}{2}$ and $\pi \leq \phi \leq 2\pi$ (see Fig. 5c). It would have been a valid assumption in the canonical problem since fields would have existed only in the exterior region of the wedge. In the rectangular cylinder problem, it should be realized that the fields do not terminate abruptly at the geometrical planes represented by dashed lines in Figs. 5a, 5b, and 5c. These dashed planes would have been occupied by the semi-infinite wedge surfaces in the canonical problems. Physically, the fields should be continuous across these dashed planes in space. Therefore, in constructing the far field as shown in (4), we have effectively created a discontinuity at each of these dashed planes. The presence of these discontinuities is solely artificial because they are created by our abrupt truncation of the fields to the regions in space corresponding to the exterior regions of the wedges used in the canonical problems. Now that the cause of the existence of the discontinuities in the far-field pattern at $\phi = 0, \frac{\pi}{2}, \pi$, and $\frac{3\pi}{2}$ has been found, we proceed to give them a physical interpretation which in turn provides a clue to their elimination.

In the following discussion, a typical case is studied and the solution to this case is derived in a step-by-step fashion. The interested reader is referred to Ko and Mittra [11] for the results of other cases.

The typical case as shown in Fig. 5a is studied. Let us concentrate on the extension of surface A. This extension is represented by a dashed line from $x = a$ to $x = \infty$ at $y = b$ in the direction $\phi = 0$. On one side of this plane, there exists H^d_{z1} as shown in Fig. 5a; on the other side there is zero field. By classical electromagnetic theory, we conclude that there is an electric surface current density existing in the dashed plane. Such a current radiates in free space to support this discontinuity in the H-field. In compact mathematical language, we write

$$\bar{J}^d_{Al} = \hat{n} \times \bar{H}^d_l = \hat{y} \times \hat{z} H^d_{zl} = \hat{x} H^d_{zl} = \hat{x} J^d_{xAl} \tag{7}$$

where $\hat{n}$ is the unit normal vector to the surface A, the subscript A refers to the extension of surface A, the subscript 1 designates the wedge under consideration, the superscript d means diffraction, and the rest should be self-explanatory. Note that a factor of 2 is not present in (7) because this J^d_{xAl} is simply the discontinuity in free space of the H-field and there is no backing by a perfect conductor in this situation.

Referring to (5) and keeping in mind that the original diffraction coefficient is perfectly valid in the direction $\phi = 0$, which implies that the procedure of subtracting the pole singularities need not concern us here, we can write

$$J^d_{xAl} = H^d_{zl}(\phi = 0)$$

$$= f_1(\phi = 0) \cdot \frac{e^{ik\rho}}{\sqrt{\rho}} \delta(y - b) \ , \ \rho \simeq x \varepsilon (a, \infty) \tag{8a}$$

where

$$f_1(\phi = 0) = e^{-ik(-a\cos\phi_0 + b\sin\phi_0)}$$

$$\cdot \frac{e^{i\frac{\pi}{4}}}{\sqrt{2\pi k}} \left[\frac{\frac{2}{3} \sin \frac{2\pi}{3} \, e^{ika}}{\cos \frac{2\pi}{3} - \cos \frac{2}{3} \phi_0} + \frac{\frac{2}{3} \sin \frac{2\pi}{3} \, e^{ika}}{\cos \frac{2\pi}{3} - \cos \frac{2}{3} \phi_0} \right] . \tag{8b}$$

Note that in the above equation, an approximation of ρ by x has been made and a constant value zero for the variable ϕ has been assumed. The far-field expression as given in (5) can be legitimately used to compute the H-field on the dashed plane because any observation points in that plane will be at least at a distance of $2a = 2\lambda$ away from the edge of wedge 1.

The H-field generated by J^d_{xAl} is

$$\bar{H}^{dEx}_{Al} = -ik \frac{e^{ik\rho} e^{i\frac{\pi}{4}}}{\sqrt{8\pi k\rho}} [-\hat{z}(-\sin\phi \tilde{J}^d_{xAl})] \tag{9}$$

where the superscript Ex stands for "excess" to remind the reader that this field has been created artificially by abruptly truncating the diffracted fields, therefore, it should not have existed; hence, the word "excess." $\tilde{J}^d_{xAl}$ in (9) is given by

$$\tilde{J}^d_{xAl} = F\{J^d_{xAl}\}$$

$$= f_1(\phi = 0) \int_{-\infty}^{\infty} \int_a^{\infty} \frac{e^{ikx}}{\sqrt{x}} \delta(y - b)\, e^{-i\alpha x}\, e^{-i\beta y}\, dxdy$$

$$= f_1(\phi = 0)\, e^{-i\beta b} \int_a^{\infty} \frac{e^{ix(k-\alpha)}}{\sqrt{x}}\, dx \quad . \tag{10}$$

By letting $x(k - \alpha) = \frac{\pi}{2} t^2$, the integral with respect to x can be transformed into an integral with respect to t which may be identified with the well-tabulated Fresnel integrals, i.e.,

$$\int_a^{\infty} \frac{e^{ix(k-\alpha)}}{\sqrt{x}}\, dx = \frac{\sqrt{2\pi}}{\sqrt{k - \alpha}} \int_{\sqrt{\frac{2a}{\pi}(k-\alpha)}}^{\infty} e^{i\frac{\pi}{2}t^2}\, dt \tag{11a}$$

$$= \frac{\sqrt{2\pi}}{\sqrt{k - \alpha}} \left[\int_0^{\infty} e^{i\frac{\pi}{2}t^2}\, dt - \int_0^{\sqrt{\frac{2a}{\pi}(k-\alpha)}} e^{i\frac{\pi}{2}t^2}\, dt \right] \tag{11b}$$

$$= \frac{\sqrt{2\pi}}{\sqrt{k}\sqrt{1 - \cos\phi}} \left[\frac{e^{i\frac{\pi}{4}}}{\sqrt{2}} - \left\{ C\left(\sqrt{\frac{2ak}{\pi}(1 - \cos\phi)}\right) + iS\left(\sqrt{\frac{2ak}{\pi}(1 - \cos\phi)}\right) \right\} \right] \tag{11c}$$

In writing (11), we have explicitly used the relation $\alpha = k \cos \phi$ and the definitions of the Fresnel integrals, i.e.,

$$C(\xi) = \int_0^{\xi} \cos\left(\frac{\pi}{2} t^2\right) dt \tag{12a}$$

and

$$S(\xi) = \int_0^{\xi} \sin\left(\frac{\pi}{2} t^2\right) dt \quad . \tag{12b}$$

Substituting (11c) in (10) and the resulting expression for $\tilde{J}^d_{xA1}$ back into (9), we have

$$\tilde{H}^{dEx}_{A1} = -ik \frac{e^{ik\rho} e^{i\frac{\pi}{4}}}{\sqrt{8\pi k\rho}} \left[-\hat{z} \left(-\sin\phi f_1(\phi = 0)\, e^{-ikb\sin\phi} \right.\right.$$

$$\left.\left. \cdot \frac{\sqrt{2\pi}}{\sqrt{k}\sqrt{1 - \cos\phi}} \left[\frac{e^{i\frac{\pi}{4}}}{\sqrt{2}} - \left\{ C\left(\sqrt{\frac{2ak}{\pi}(1 - \cos\phi)} \right) + iS\left(\sqrt{\frac{2ak}{\pi}(1 - \cos\phi)} \right) \right\} \right] \right) \right] \tag{13}$$

where $f_1(\phi = 0)$ is given in (8b).

Now we have the expression for the field generated by J^d_{xA1} as shown in (13). The next step is to examine the discontinuity introduced at $\phi = 0$ by $\tilde{H}^{dEx}_{A1}$. To this end, all we need to pay attention to is the following limit:

$$\lim_{\phi \to \begin{Bmatrix} 0 \\ 2\pi \end{Bmatrix}} \frac{\sin\phi}{\sqrt{1 - \cos\phi}} = \lim_{\phi \to \begin{Bmatrix} 0 \\ 2\pi \end{Bmatrix}} \frac{2 \sin\frac{\phi}{2} \cos\frac{\phi}{2}}{\sqrt{2} \sin\frac{\phi}{2}} = \begin{Bmatrix} \sqrt{2} \\ -\sqrt{2} \end{Bmatrix} \quad . \tag{14}$$

Using (14) and (13), the discontinuity introduced at $\phi = 0$ by $\tilde{H}^{dEx}_{A1}$ is found to be

$$\bar{H}_{A1}^{dEx}(\phi = 0) - \bar{H}_{A1}^{dEx}(\phi = 2\pi)$$

$$= -ik \frac{e^{ik\rho} e^{i\frac{\pi}{4}}}{\sqrt{8\pi k\rho}} \left[-\hat{z} \left(-[\sqrt{2} - (-\sqrt{2})]\, f_1(\phi = 0) \cdot \sqrt{\frac{2\pi}{k}}\ \frac{e^{i\frac{\pi}{4}}}{\sqrt{2}} \right) \right]$$

$$= \hat{z}\, \frac{e^{i\frac{\pi}{4}}}{\sqrt{2}} \frac{e^{ik\rho}}{\sqrt{\pi k\rho}} \left[e^{-ik(-a\cos\phi_0 + b\sin\phi_0)}\ \frac{(2)(\frac{2}{3}\sin\frac{2\pi}{3}) e^{ika}}{\cos\frac{2\pi}{3} - \cos\frac{2}{3}\phi_0} \right] . \qquad (15)$$

It is indeed enlightening to see that this discontinuity is exactly the discontinuity given in (6). The study of the typical case is now completed. For the cases depicted in Figs. 5a, 5b, and 5c, the interested reader is referred to Ko and Mittra [11].

Before closing this section, it is worthwhile to recapitulate the main points discussed. The discontinuities at $\phi = 0$, $\frac{\pi}{2}$, π, and $\frac{3\pi}{2}$ in the far-field pattern obtained by the GTD technique have been shown to be caused by the abrupt truncation of the diffracted field which is effectively equivalent to artificially introducing sheets of electric surface current in free space. When these current sheets radiate strongly in the directions $\phi = 0$, $\frac{\pi}{2}$, π, and $\frac{3\pi}{2}$, they produce discontinuities corresponding exactly to those in the GTD far-field pattern. This discovery provides us with a clue to further improve the GTD far-field pattern. One simply subtracts out all these artificially created "excess" fields from the GTD far-field pattern to eliminate these discontinuities. The improved GTD far-field pattern is discussed in the next section along with some comparisons with the conventional moment method solution and results obtained by a GTD-moment method hybrid technique [1] and a self-consistent method [12].

3. IMPROVED FAR-FIELD PATTERN AND COMPARISON WITH RESULTS OBTAINED BY OTHER APPROACHES

In the last section, Keller's wedge diffraction coefficient was used to construct the far field scattered by a rectangular cylinder. It was shown that when the pole singularities contained in the physical optics current with infinite support on the semi-infinite wedge surface were subtracted from the wedge diffraction coefficient, the far field remained finite and varied smoothly across the geometrical optics shadow and reflection boundaries. Other than the noticeable discontinuities in the directions in which the surfaces of the rectangular cylinder are oriented, that far-field pattern was in fair agreement with the conventional moment method solution.

It was pointed out that these discontinuities were caused by abrupt truncations of the diffracted field to the regions in space which correspond to the exterior regions in the wedge canonical problems. These abrupt truncations were demonstrated to be effectively equivalent to artificial introductions of semi-infinite electric surface current sheets in free space. An in-depth study of these current sheets consequently showed that they radiated strongly and introduced identical discontinuities in those directions corresponding to the discontinuities in the GTD far field. This discovery provides a clue which leads to further improvement of the GTD far-field pattern.

The elimination of these discontinuities can be achieved by subtracting $\bar{H}_{A1}^{dEx}$, $\bar{H}_{D1}^{dEx}$, $\bar{H}_{A2}^{dEx}$, $\bar{H}_{B2}^{dEx}$, $\bar{H}_{B3}^{dEx}$, and $\bar{H}_{C3}^{dEx}$, obtained in the last section, from the GTD H_z^d given in (4). The improved GTD far-field pattern so obtained is displayed in Fig. 6. It is very interesting to observe that not only the discontinuities at $\phi = 0$, $\frac{\pi}{2}$, π, and $\frac{3\pi}{2}$ disappear completely, but also that nulls, which were not present in the GTD far-field pattern in Fig. 4, are showing up in the neighborhood of $\phi = \pi$ and $\phi = \frac{3\pi}{2}$. The disappearance of

the discontinuities is to be expected since these discontinuities have been examined carefully in the last section and were shown to be identical to those in the GTD far-field pattern in Fig. 4.

Finally, results obtained by using (a) the conventional moment method [2] with 32 unknowns, (b) the hybrid moment method and GTD technique by Burnside et al. [1] with 24 unknowns, and (c) the self-consistent method [12] with 8 unknowns are exhibited in Fig. 7. Note that in Fig. 7, the self-consistent method, which uses *all* higher-order multiple-edge interactions in its formulation, still does not eliminate the discontinuities at $\phi = 0°$, 90°, 180°, and 270°. While the conventional moment method solution and the moment method-GTD hybrid solution deviate only slightly in the backscattering direction, the present method solution as shown in Fig. 6 is in good agreement with them.

4. ACCURACY CHECK

In the previous sections, a method has been discussed for obtaining an improved scattered far-field pattern of a perfectly conducting rectangular cylinder illuminated by a plane wave whose magnetic intensity vector is parallel to the axis of the cylinder. The resulting improved scattered far-field pattern has been compared with results obtained by other approaches in the literature. In particular, results obtained by using (a) the conventional moment method [2] with 32 unknowns, (b) the hybrid moment method and GTD technique by Burnside et al. [1] with 24 unknowns, and (c) the self-consistent method [12] with 8 unknowns have been used for comparisons.

Out of these three different approaches, only the conventional moment method has *consistently* taken into account in its formulation the boundary condition, requiring the tangential components of the total electric field to be vanished on the surface of the rectangular cylinder. In Burnside's

hybrid moment method and GTD technique, the boundary condition is not enforced on the entire surface of the scattering object, as in the case of the conventional moment method. Instead, point matching is applied at the midpoint of each of the pulse current segments, located near the diffracting edges of the wedges of the rectangular cylinder, and at some arbitrary points in the GTD regions of the surface of the rectangular cylinder, in order to obtain an equal number of equations as the involved unknowns including the current samples and the diffraction constants. The final result is somewhat dependent on the locations of the arbitrarily chosen additional matching points in the GTD region on the surface of the scatterer. In the self-consistent method, no consideration is given to the satisfaction of the boundary condition.

Although the comparisons of the scattered far-field pattern with those obtained by the aforementioned methods are very favorable, indicating the solutions are in good agreement with the true solution, an independent accuracy check must be applied to further validate the approximate solution, especially when there are no available results in the literature to compare with. Such an accuracy check is often needed but is not readily available in other high-frequency asymptotic techniques.

In this section, we present a method which allows us to calculate the tangential components of the scattered electric field on the surface of the scatterer using the approximate scattered far-field pattern. The accuracy of the solution can then be checked simply by observing whether these tangential components of the scattered electric field on the surface of the scatterer are equal to the negative of the tangential components of the incident electric field on the surface of the scatterer. If the outcome of such an observation is favorable, then the solution is good; otherwise, further improvement is needed.

4.1 Method of computation

In classical electromagnetic theory, it is well-known that the scattered magnetic far field is related to the Fourier transform of the scattered electric field on an aperture in a relatively simple manner. Consider the aperture shown in Fig. 8. This aperture is a plane at y = b, containing the surface of the rectangular cylinder as its central portion. The scattered far-field pattern enclosed in the hemisphere corresponding to this aperture as shown in Fig. 8 is used to compute the Fourier transform of the scattered electric field on the aperture. In particular, for the H-wave case considered in this paper, the Fourier transform of the tangential component of the scattered electric aperture field can be written as

$$\tilde{E}^{s}_{xAP}(\phi) = \frac{Z_0}{ik} \cdot \frac{1}{2g(\rho)} \cdot T^{H}(\phi) \cdot \exp(-ikb \sin \phi) \tag{16}$$

where

$$g(\rho) = \frac{e^{ik\rho + i\frac{\pi}{4}}}{\sqrt{8\pi k\rho}}$$

Z_0 is the free-space characteristic impedance

$T^{H}(\phi)$ is that portion of the scattered magnetic far-field pattern enclosed in the proper hemisphere corresponding to the aperture under consideration, and

ρ and ϕ are the polar coordinates.

The phase factor in (16) is to assure that the aperture at y = b, but not at y = 0, is under consideration. The tangential scattered electric aperture field in the space domain can be obtained readily by an inverse Fourier transform, viz.,

$$E^{s}_{xAP}(x, y = b) = F^{-1}\{\tilde{E}^{s}_{xAP}[\phi(\alpha)]\} \quad . \tag{17}$$

The tangential scattered electric aperture field in (17) is truncated to the surface of the scatterer, i.e., $x \in [-a,a]$, and an observation can be made to judge whether the tangential scattered electric field on the surface of the rectangular cylinder is indeed equal to the tangential incident electric field.

The hemisphere shown in Fig. 8 is for the aperture at $y = b$. Similar hemispheres and apertures corresponding to the other surfaces of the rectangular cylinder can be established and the tangential components of the scattered electric field on these surfaces can be computed in a similar fashion.

4.2 Results and comments

In the previous sections, an improved scattered magnetic far-field pattern has been obtained (see Fig. 6). The accuracy of that pattern can be verified by computing the tangential component of the scattered electric field on the surface of the rectangular cylinder using the method outlined in Subsection 4.1. The resulting tangential component of the scattered electric field on the surface — $x \in [-a,a]$, $y = b$ — is shown in Figs. 9a and 9b. These curves were obtained by using that portion of the improved pattern (Fig. 6) enclosed in the hemisphere schematically indicated in Fig. 8, and by using the one-dimensional FFT for the inverse Fourier transform operation.

The magnitude of the tangential scattered E-field shown in Fig. 9a oscillates around the constant value 266.58, which is the magnitude of the tangential component of the incident E-field. More precisely, for normalized H-wave incidence, $|H^i| = 1$, $|E^i| = 377$, and the incident angle $\phi_0 = 45°$; therefore, the magnitude of the tangential component of the incident E-field is $|E^i \cos 45°| = 266.58$. The phase of the tangential scattered E-field shown in Fig. 9b is varying linearly across the surface of the rectangular cylinder and can be readily verified to be of a phase difference of π or 180° from the phase of the tangential incident E-field on the surface. Similar behaviors

of the tangential scattered E-field on other surfaces of the rectangular cylinder can be obtained and are not repeated here. These observations confirm that the improved far-field pattern obtained in the last section is indeed a very good approximation to the true scattered field. Of course, the comparisons with results obtained by other approaches as done in the previous section not only further validate the approximate solution, but also demonstrate the effectiveness of the accuracy checking method developed in this section.

5. SUMMARY

In this paper, the scattered far-field pattern of a perfectly conducting rectangular cylinder illuminated by a plane H-wave has been obtained by a zeroth-order GTD approximation and the result improved by a straightforwardly physical interpretation of the existence of the discontinuities in the zeroth-order GTD far-field pattern.

The improved scattered far-field pattern has been compared with results obtained by other different approaches and the similarities and differences between these results have been discussed. Generally speaking the improved pattern obtained by the present approach is in good agreement with the conventional moment-method solution with 32 unknowns.

An accuracy checking method has also been presented so that an independent check on the satisfaction of the boundary condition on the surface of the rectangular cylinder can be performed. The results of such an accuracy check are quite favorable, which demonstrates that the improved far-field pattern obtained by the present approach is indeed a close approximation to the true solution. The merit of such an independent accuracy checking scheme is that the approximate solution obtained can be validated without making

comparisons with other methods. Although not needed here, the spectral approach to diffraction can be employed in conjunction with the integral equation for the surface current to systematically improve the solution where such an improvement is needed.

ACKNOWLEDGEMENT

The work reported herein was sponsored in part by the Joint Services of Electronics Program under Grant DAAB-07-72-C-0259 and in part by the Army Research Office under Grant ARO-DAAG-29-77-G-0111.

REFERENCES

[1] W. D. Burnside, C. L. Yu and R. J. Marhefka, "A technique to combine the geometrical theory of diffraction and the moment method," IEEE Trans. Antennas Propagat., vol. AP-23, pp. 551-558, July 1975.

[2] K. K. Mei and J. G. Van Bladel, "Scattering by perfectly-conducting rectangular cylinders," IEEE Trans. Antennas Propagat., vol. AP-11, pp. 185-192, March 1963. Also see corrections.

[3] J. R. Mautz and R. F. Harrington, "Radiation and scattering from large polygonal cylinders, transverse electric fields," Scientific Report No. 7, AFCRL-TR-75-0343, Department of Electrical and Computer Engineering, Syracuse University, Syracuse, New York, June 1975.

[4] M. F. Iskander and M. A. K. Hamid, "Scattering by a regular polygonal conducting cylinder," to appear.

[5] R. G. Kouyoumjian and N. Wang, "Diffraction by a perfectly conducting rectangular cylinder which is illuminated by an array of line sources," Report 3001-7, Electro-Science Laboratory, Department of Electrical Engineering, Ohio State University, Columbus, Ohio, prepared under Grant NGR 36-008-144 for NASA, August 1973.

[6] J. H. Richmond, "An integral-equation solution for TE radiation and scattering from conducting cylinders," Research Report, Electro-Science Laboratory, Ohio State University, Columbus, Ohio, April 1973.

[7] R. G. Kouyoumjian and P. H. Pathak, "A uniform geometrical theory of diffraction for an edge in a perfectly-conducting surface," Proc. IEEE, vol. 62, pp. 1448-1461, November 1974.

[8] R. M. Lewis, D. S. Ahluwalia and J. Boersma, "Uniform asymptotic theory of diffraction by a plane screen," SIAM J. Appl. Math., vol. 16, pp. 783-807, 1968.

[9] R. Mittra, Y. Rahmat-Samii and W. L. Ko, "Spectral theory of diffraction," Appl. Phys., vol. 10, pp. 1-13, 1976.

[10] W. L. Ko and R. Mittra, "A new approach based on a combination of integral equation and asymptotic techniques for solving electromagnetic scattering problems," IEEE Trans. Antennas Propagat., vol. AP-24, March 1977 (in press).

[11] W. L. Ko and R. Mittra, "A method for combining integral equation and asymptotic techniques for solving electromagnetic scattering problems," Electromagnetics Lab Report 76-6, Tech. Report, prepared under Contracts DAHC04-74-G-0113 and N00014-75-C-0293, May 1976.

[12] J. S. Yu and R. C. Rudduck, "On higher-order diffraction concepts applied to a conducting strip," IEEE Trans. Antennas Propagat., vol. AP-15, pp. 662-668, September 1967.

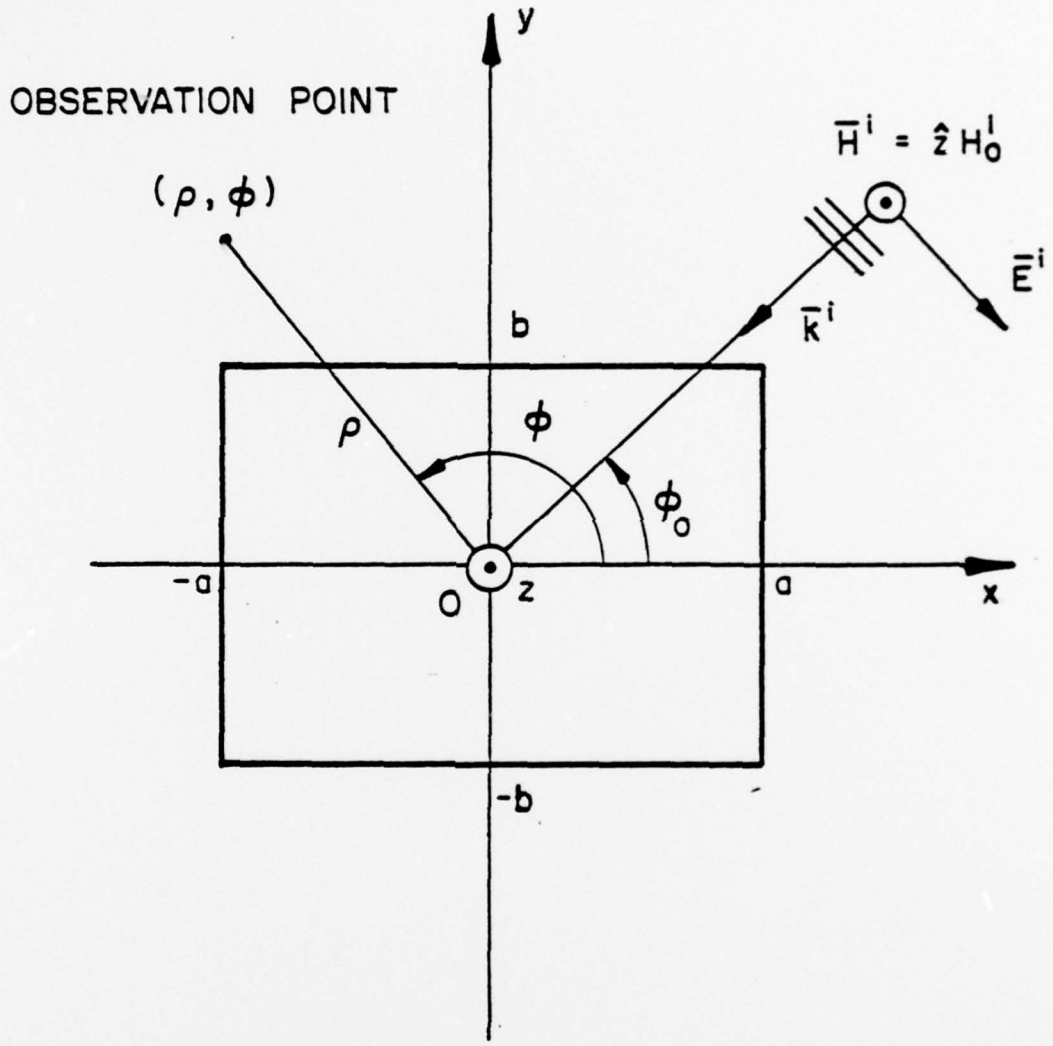

Fig. 1. Diffraction by a rectangular cylinder illuminated by an H-polarized plane wave incident at an angle ϕ_0.

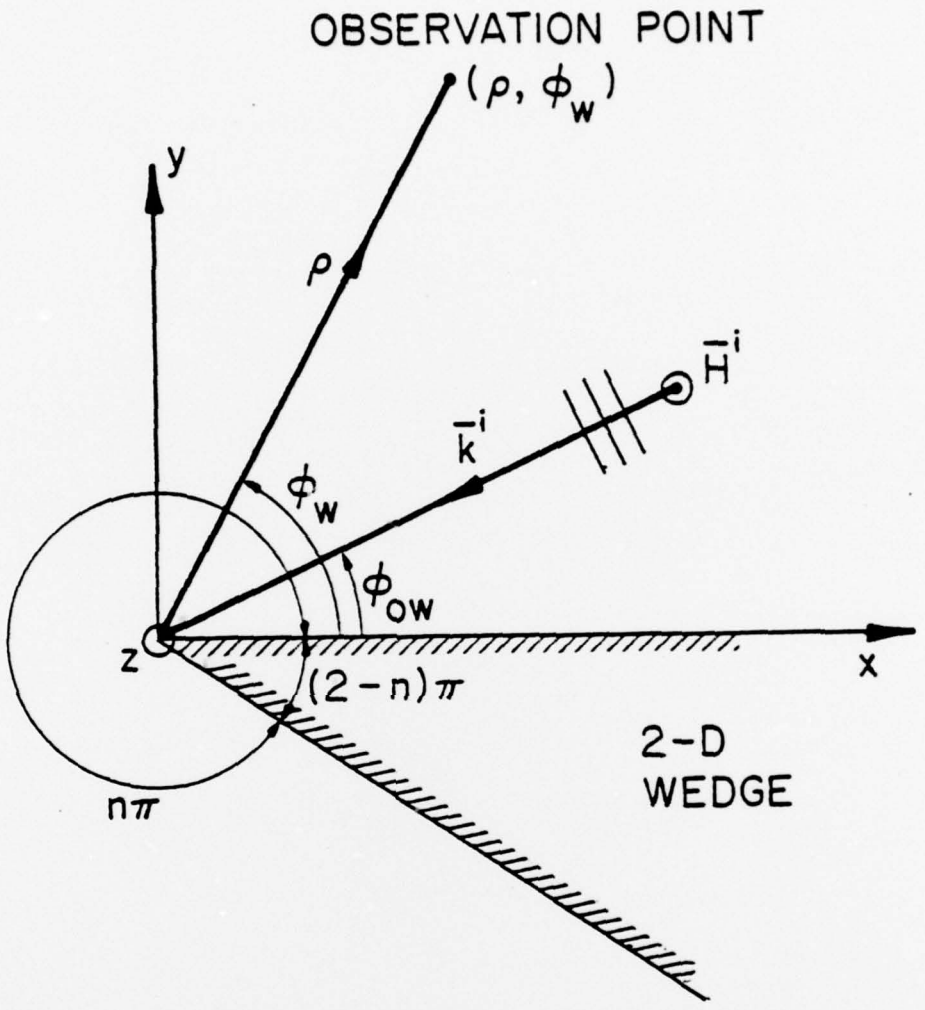

Fig. 2. Geometry of a perfectly conducting wedge immersed in a uniform H-wave in the canonical wedge diffraction problem.

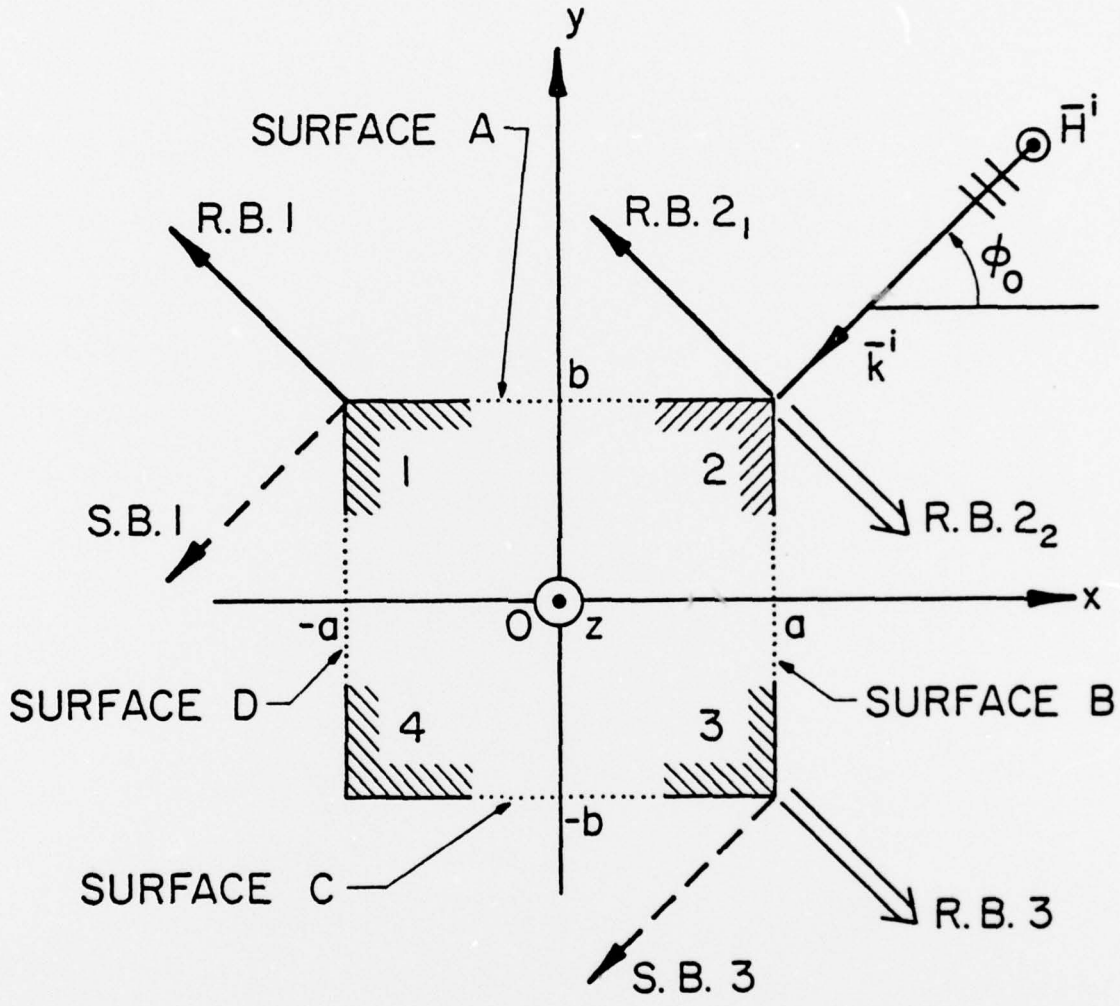

Fig. 3. For the angle of incidence ϕ_0 as shown, wedges 1, 2, and 3 are illuminated while wedge 4 is in the dark.

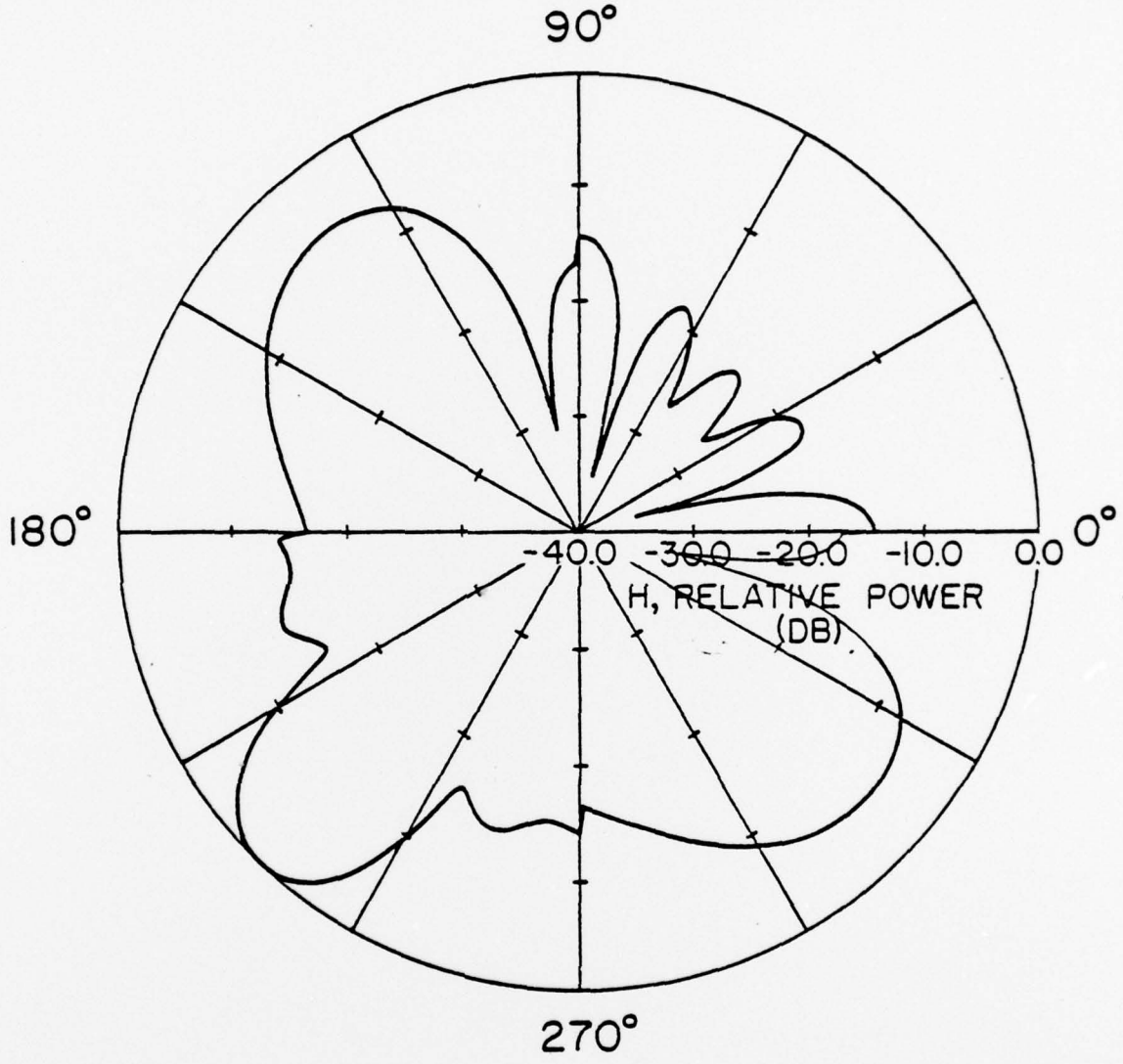

Fig. 4. Diffracted far-field pattern of the rectangular cylinder obtained by using (4); $\phi_0 = \pi/4$, $a = b = 1\lambda$.

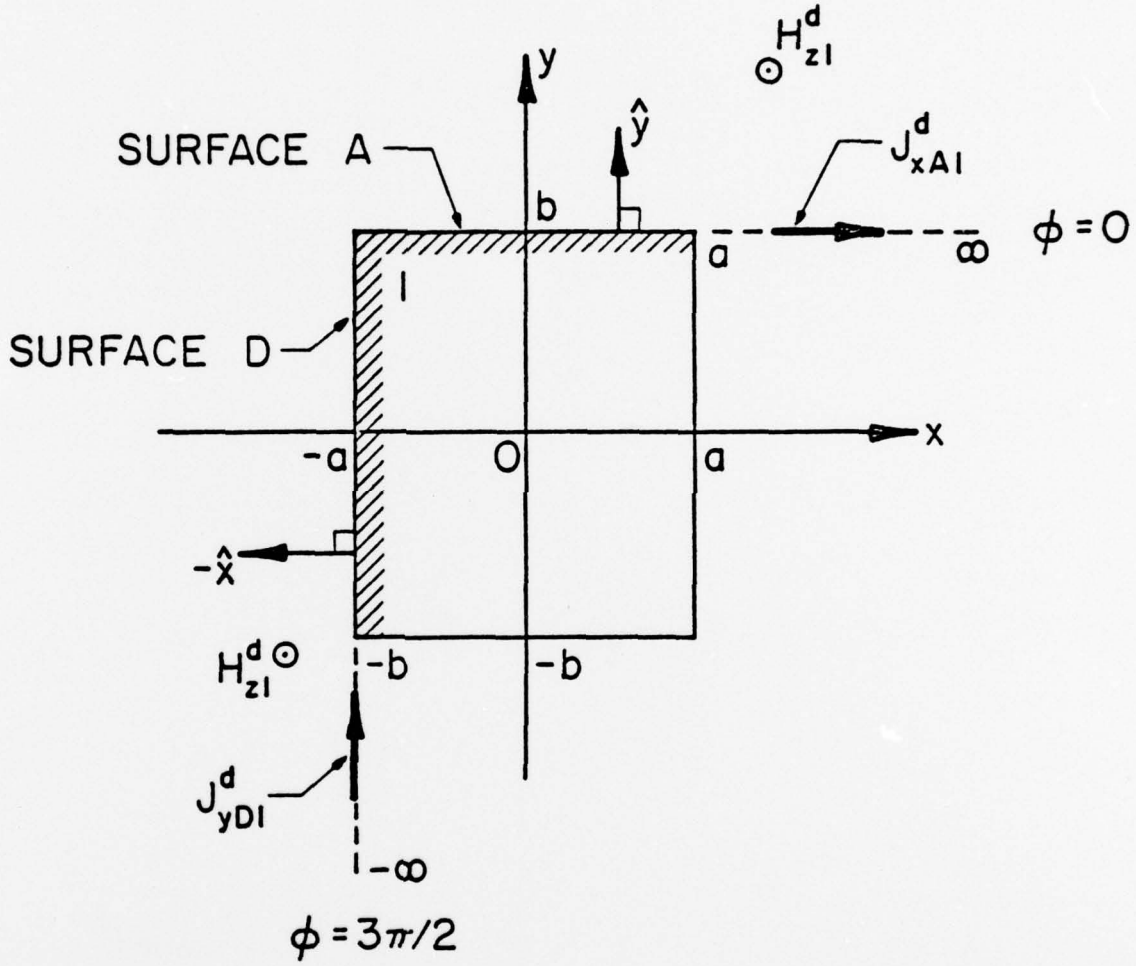

Fig. 5a. J^d_{yD1}, J^d_{xA1} contribute to the discontinuities in the far field at $\phi = \frac{3\pi}{2}$, $\phi = 0$, respectively.

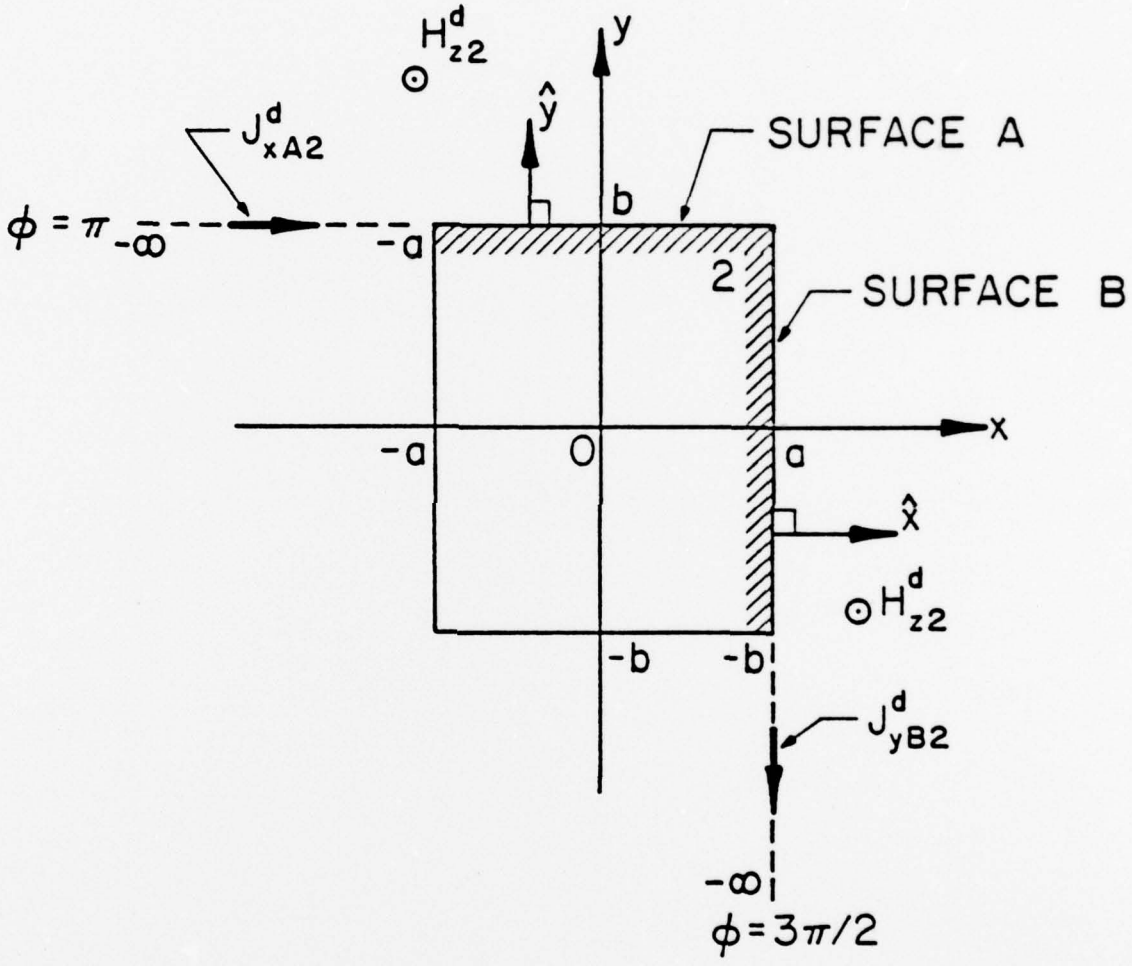

Fig. 5b. J^d_{yB2}, J^d_{xA2} contribute to the discontinuities in the far field at $\phi = \frac{3\pi}{2}$, $\phi = \pi$, respectively.

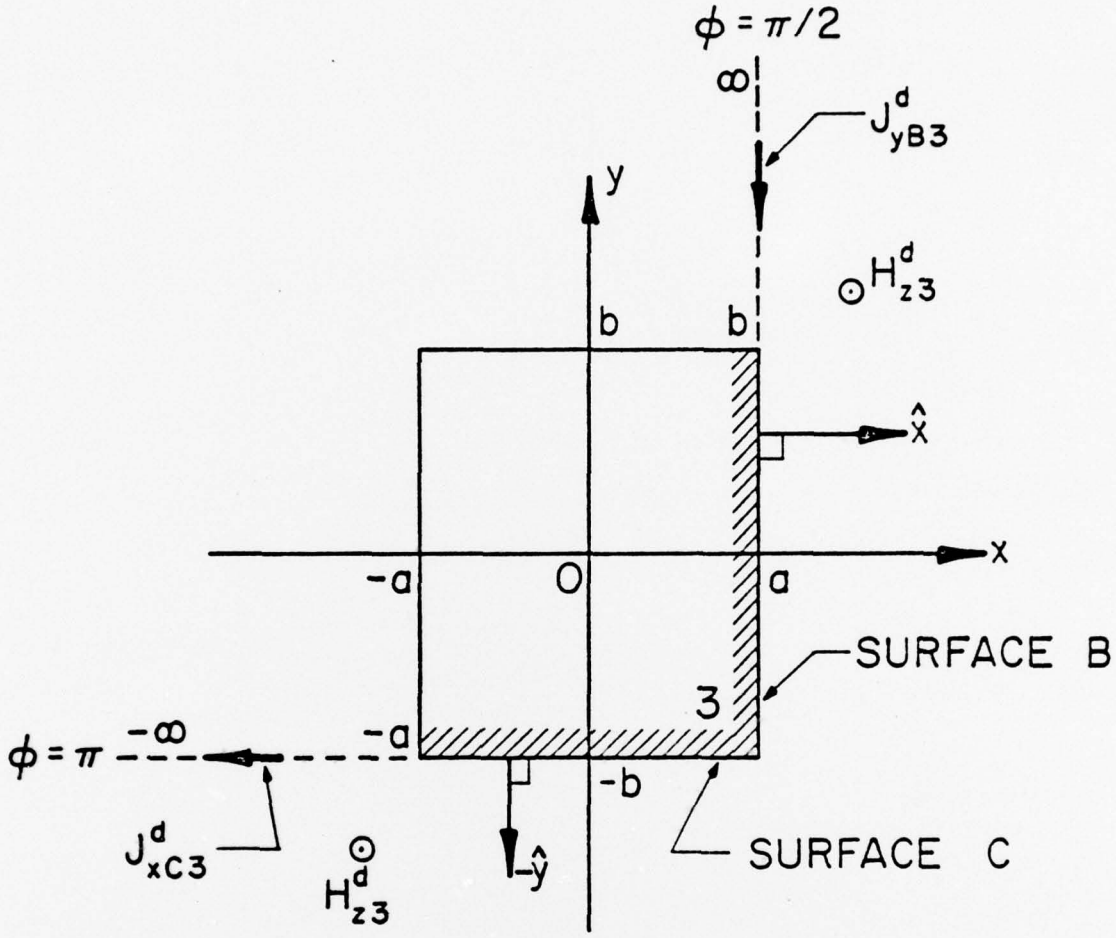

Fig. 5c. J^d_{xC3}, J^d_{yB3} contribute to the discontinuities in the far field at $\phi = \pi$, $\phi = \frac{\pi}{2}$, respectively.

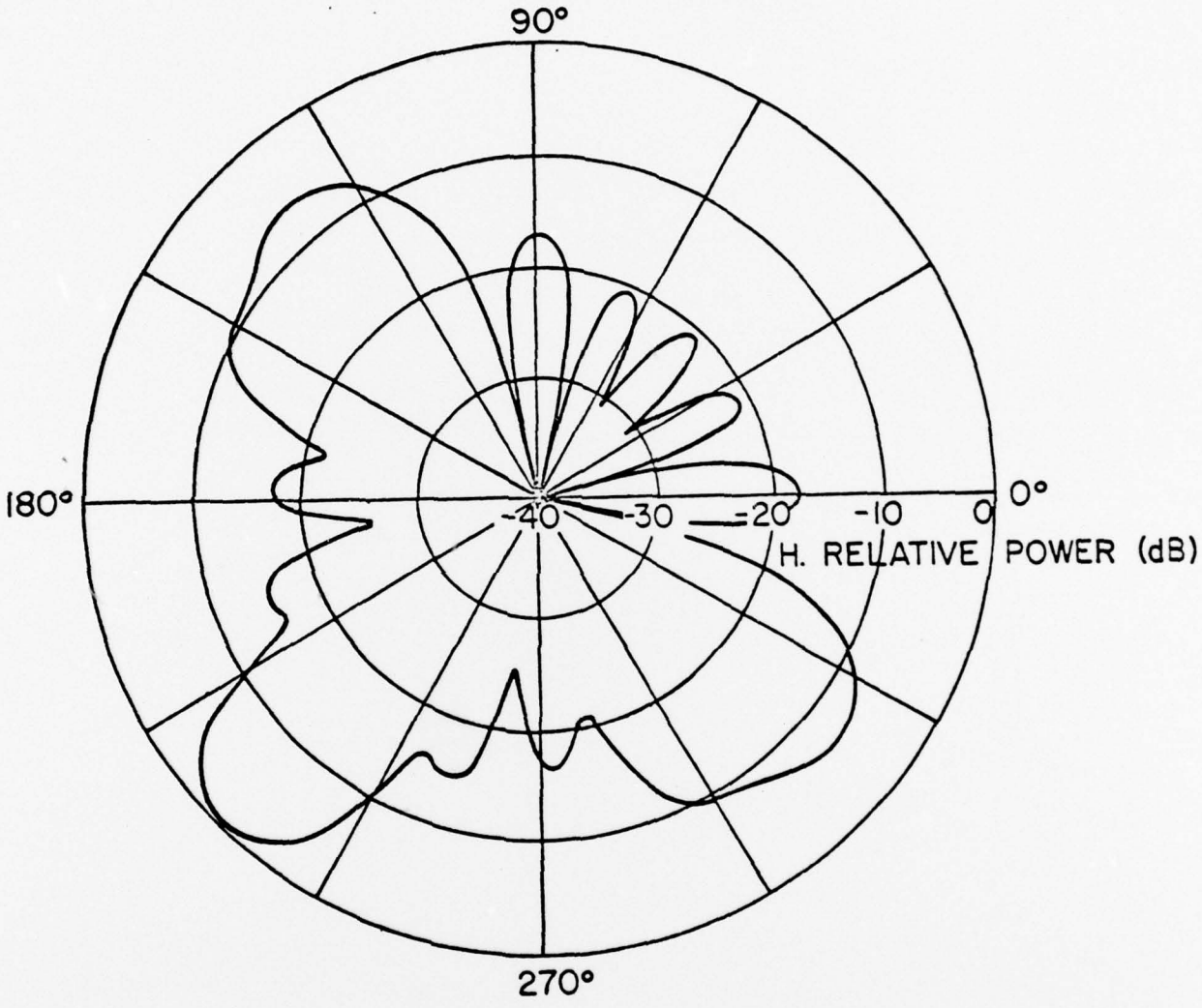

Fig. 6. Improved scattered far-field pattern of the rectangular cylinder; $\phi_0 = \pi/4$, $a = b = 1\lambda$.

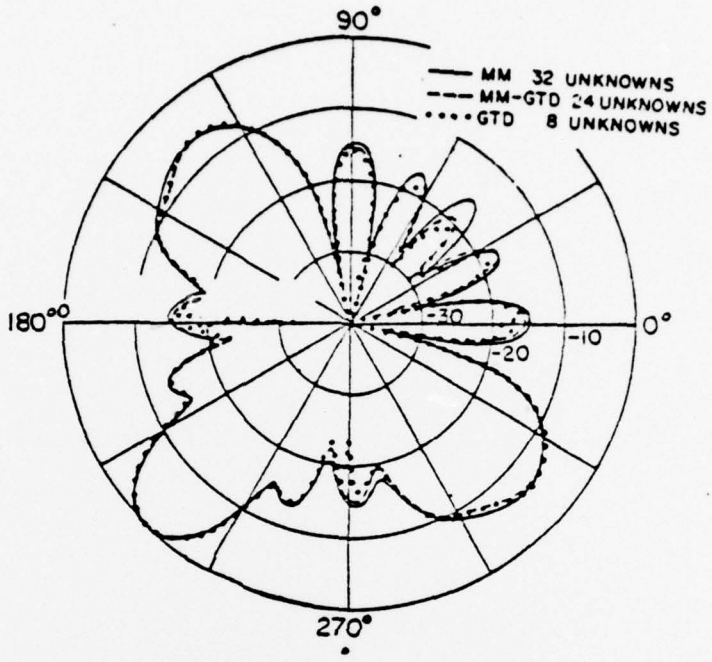

Fig. 7. db plot of scattered far-field patterns for the rectangular cylinder calculated by using the moment method, GTD and hybrid technique; $\phi_o = \pi/4$, $a = b = 1\lambda$.

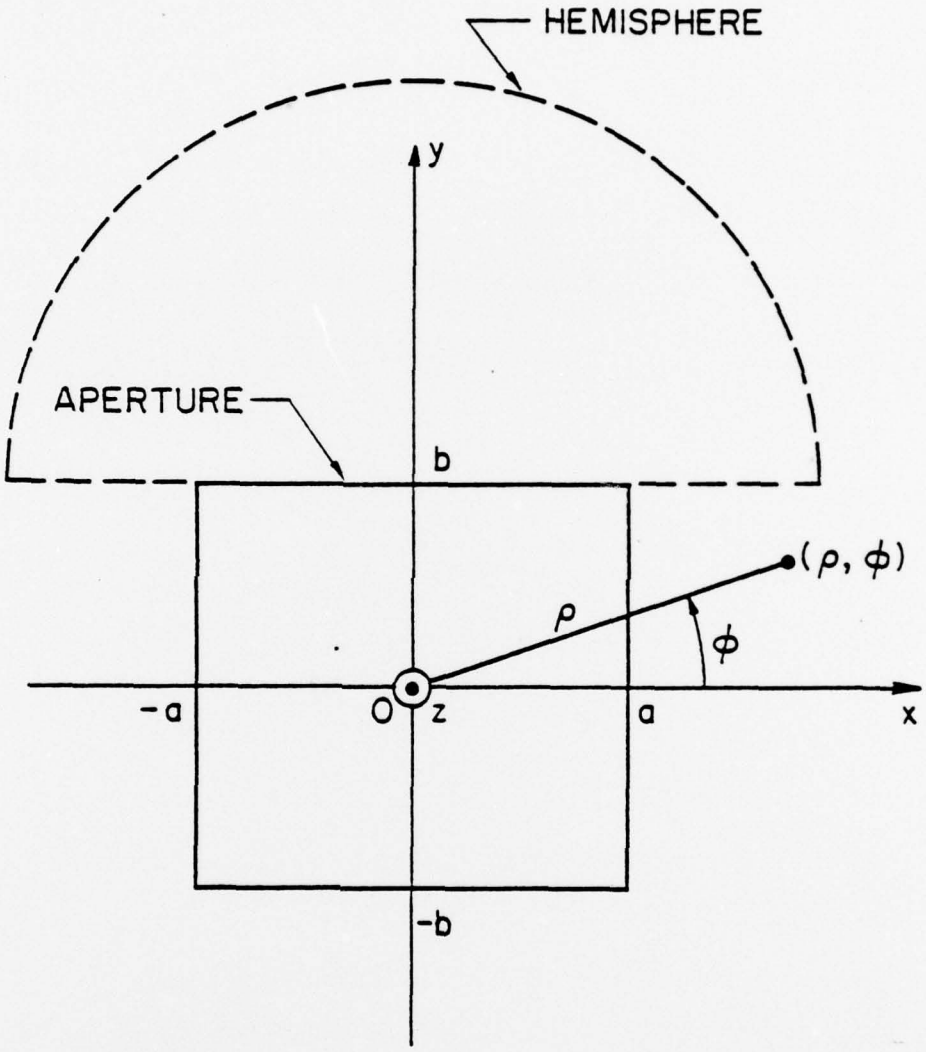

Fig. 8. Scattered far-field pattern in the hemisphere is used to obtain the scattered E-field on the aperture.

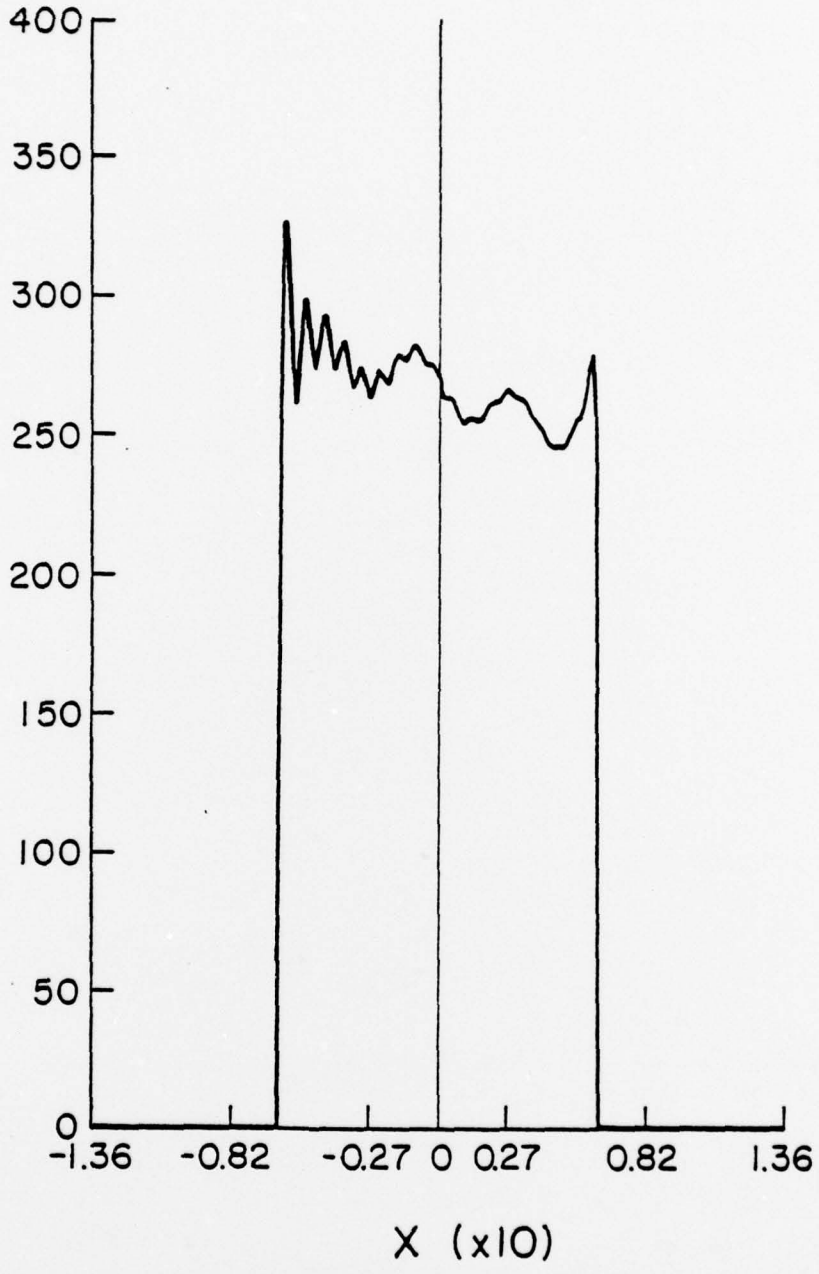

Fig. 9a. Magnitude of the scattered E-field on the aperture shown in Fig. 8, truncated to the surface of the rectangular cylinder.

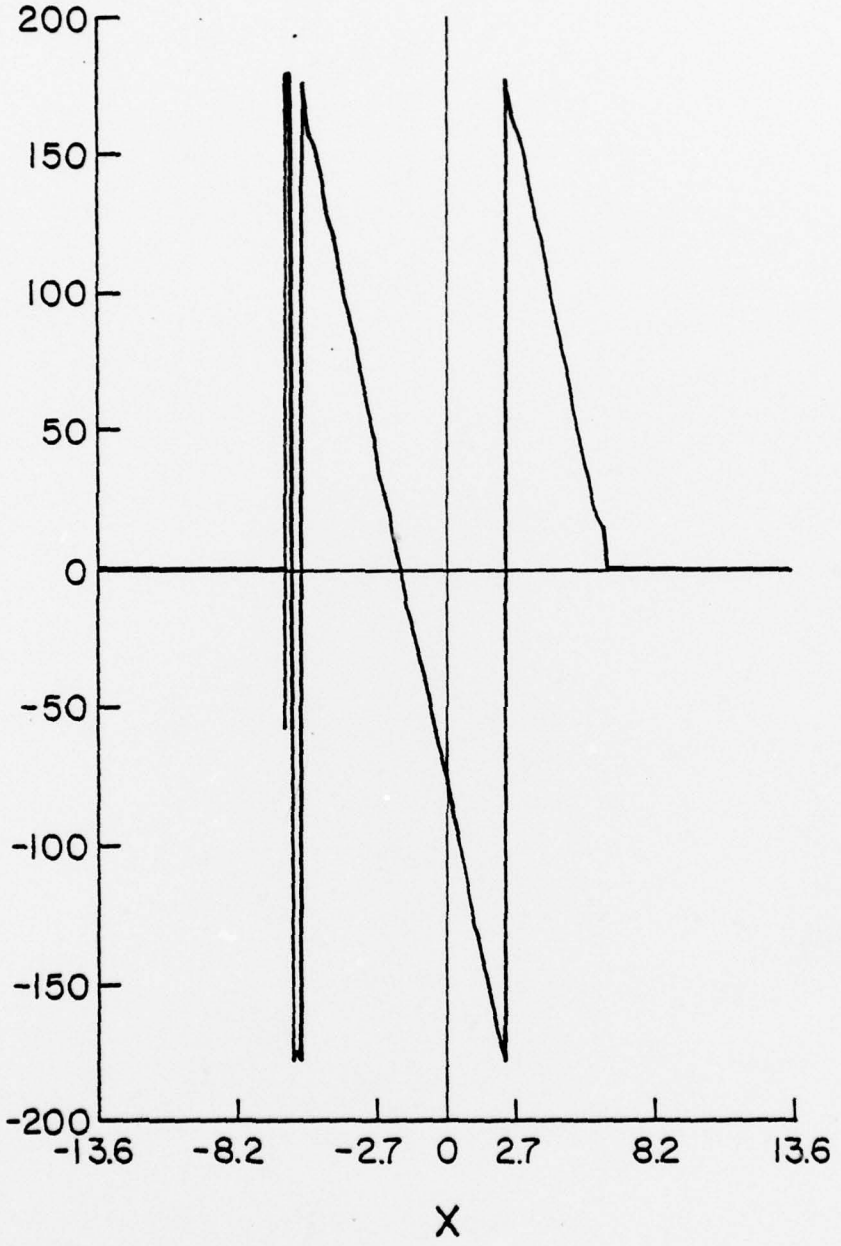

Fig. 9b. Phase of the scattered E-field on the aperture shown in Fig. 8, truncated to the surface of the rectangular cylinder.